

# PMC-InterCPT: Rethinking Biomedical Interleaved Data for Multimodal Continued Pretraining

Guanghao Zhu<sup>1</sup> Zeyu Liu<sup>1</sup> Zhitian Hou<sup>2</sup> Pengkai Wang<sup>1</sup> Zhijie Sang<sup>3</sup>  
Minheng Ni<sup>1</sup> Wenjun Wang<sup>1</sup> Yanggan Gu<sup>1</sup> Shuo Cai<sup>1</sup> Congkai Xie<sup>3</sup>  
Jianmin Wu<sup>1,4</sup> Hongxia Yang<sup>1,3,4\*</sup>

<sup>1</sup>The Hong Kong Polytechnic University

<sup>2</sup>Sun Yat-sen University

<sup>3</sup>InfiX.ai

<sup>4</sup>PolyU-Daya Bay Technology and Innovation Research Institute

## Abstract

Large-scale biomedical image-text datasets extracted from scientific literature provide valuable resources for medical multimodal model training. These datasets are commonly organized as image-caption pairs; however, figure captions are often short, context-dependent, and only partially informative without the surrounding article text. At the same time, large-scale automatic extraction introduces structural noise such as missing captions, residual markup, duplicated context, and incoherent multi-paragraph figure descriptions. We revisit data construction for medical multimodal continued pretraining (CPT) and present PMC-InterCPT, a context-grounded biomedical interleaved corpus that incorporates figure-referencing body text in addition to captions. Our pipeline recovers missing captions, cleans caption and context text, reconstructs coherent interleaved image-text samples, and applies LLM-supervised medical relevance and quality classifiers to filter noisy records. We further reveal strong modality imbalance in the resulting corpus and introduce a four-bucket evidence taxonomy for modality-aware resampling. Through CPT followed by supervised fine-tuning (SFT) on Qwen3.5-4B-Base, PMC-InterCPT effectively improves medical and general multimodal performance while using fewer CPT tokens than the raw source pool. The experimental results also illustrate the complementarity between the data quality and modality for medical multimodal CPT.

## 1 Introduction

Multimodal large language models (MLLMs) have achieved remarkable progress across a wide range of tasks, driven by large-scale multimodal pretraining data (Radford et al., 2021; Chen et al., 2022). In the biomedical domain, such progress holds particular promise: integrating visual and textual

knowledge across medical specialties could support clinical decision-making, accelerate research, and improve diagnostic workflows (Lozano et al., 2025). A key enabler of this vision is the availability of large-scale, high-quality medical multimodal training data, particularly *interleaved* image-text data that preserves the rich in-context descriptions of figures found in scientific articles.

Lozano et al. (2025) introduced BIOMEDICA, currently the largest open biomedical image-text resource, comprising over 24 million image-text pairs extracted from the PubMed Central Open Access subset. BIOMEDICA provides extensive metadata and image-level annotations, and has been used to train state-of-the-art biomedical CLIP-style models. However, the dataset was constructed with image-caption pairs as the primary output format. This design choice leaves a substantial source of training signal untapped: the body-text paragraphs that inline-reference each figure typically provide richer, more context-dependent descriptions than captions alone. Moreover, we identify several categories of structural noise introduced by BIOMEDICA’s automatic extraction pipeline and figure-level pair organization: (1) missing captions that can be recovered from PMC XML; (2) residual inline XML markup and short-sentence or near-duplicate repetition in captions and contexts; (3) repeated context strings attached to multiple figures or duplicate PMC records; and (4) multi-figure context aggregation noise, where body paragraphs shared across multiple figures are redundantly attached to each figure independently.

In this work, we address these limitations by proposing a systematic pipeline for cleaning and reconstructing *context-grounded interleaved image-text data* from BIOMEDICA. Our pipeline recovers missing captions from PMC XML, removes residual markup and repeated text/context, constructs interleaved samples that pair images with their figure-specific body-text context, refines non-contiguous

\*Corresponding author.  
hongxia.yang@polyu.edu.hk.

Email:

context sequences, and applies LLM-supervised medical relevance and quality classifiers to filter out non-medical and low-quality samples. We refer to the resulting dataset as PMC-InterCPT, a quality-filtered and modality-balanced interleaved corpus for medical multimodal continued pretraining (CPT). We further analyze the resulting data distribution and observe severe modality imbalance. Plots and Charts alone account for 53.7% of tokens in the medical quality-filtered data, while clinically relevant categories such as Clinical Imaging represent only 7.3%. To address this, we propose a taxonomy of four *evidence buckets* and conduct systematic experiments on modality-aware resampling strategies.

We evaluate our approach through CPT plus supervised fine-tuning (SFT) experiments on Qwen3.5-4B-Base across medical, scientific, and general multimodal benchmarks. Our experiments show that PMC-InterCPT improves over full raw BIOMEDICA and that modality-aware resampling provides a useful medical-general tradeoff.

Our main contributions are:

- A systematic pipeline for cleaning and reconstructing context-grounded interleaved biomedical CPT data from BIOMEDICA, addressing caption errors, context noise, and sample construction quality.
- PMC-InterCPT, a high-quality medical multimodal CPT dataset of approximately 9.63B tokens (quality  $\geq 1$ , modality-balanced), with a four-bucket evidence taxonomy for principled resampling.
- Comprehensive CPT experiments on Qwen3.5-4B-Base demonstrating that data quality and modality distribution are two orthogonal, complementary dimensions for medical multimodal CPT optimization.

## 2 Related Work

### 2.1 Medical Multimodal Large Language Models

Recent years have witnessed rapid development of medical multimodal large language models (MLLMs), including LLaVA-Med (Li et al., 2023), Med-Flamingo (Moor et al., 2023), HuatuoGPT-Vision (Chen et al., 2024), MAIRA-2 (Bannur et al., 2024), and LingShu (Xu et al., 2025), which adapt

general-purpose VLMs to clinical and biomedical domains through instruction tuning or domain-adaptive pretraining. Despite strong performance on medical VQA tasks, these models typically rely on small curated instruction datasets or general-domain pretrained weights, without access to large-scale high-quality medical interleaved CPT data. Our work addresses this gap by constructing and validating a CPT dataset specifically designed for this purpose.

### 2.2 Biomedical Multimodal Datasets from Scientific Literature

Several large-scale datasets have been constructed from PubMed Central, including PMC-15M (Zhang et al., 2023a), Open-PMC-18M (Baghbanzadeh et al., 2025), and BIOMEDICA (Lozano et al., 2025). These datasets vary in scale, modality coverage, and extraction methodology, but share a common design: image-caption pairs as the primary output. Open-PMC-18M further incorporates subfigure extraction and contextual text enrichment, and demonstrates that precise data curation and alignment outweigh scale for representation learning (Baghbanzadeh et al., 2025). Our work builds on BIOMEDICA and extends it by constructing interleaved samples from body-text context, with systematic noise removal and quality filtering tailored for CPT.

### 2.3 Interleaved Image-Text Pretraining

Flamingo (Alayrac et al., 2022) demonstrated that interleaved image-text data enables strong few-shot multimodal generalization. Subsequent work including MMC4 (Zhu et al., 2023) and OBELICS (Laurençon et al., 2023) scaled interleaved web data to billions of documents, showing consistent benefits over image-caption pair training. Construction of medical-domain interleaved data remains largely unexplored; our work systematically builds and validates such data from biomedical scientific literature.

### 2.4 Data Quality and Mixture for Pretraining

FineWeb (Penedo et al., 2024), DCLM (Li et al., 2024b), and RefinedWeb (Penedo et al., 2023) have established that careful quality filtering of web text yields substantial gains for general LLM pretraining. DoReMi (Xie et al., 2023) showed that domain reweighting can significantly accelerate pretraining convergence. We extend these principles to medical multimodal CPT by combining LLM-based quality

filtering with a novel modality-aware resampling strategy, and provide a systematic empirical study of their effects in this setting.

### 3 Data Construction Pipeline

BIOMEDICA provides a large-scale collection of biomedical image-text pairs extracted from the PubMed Central Open Access subset. While it offers significant scale and rich metadata, the automatic extraction process and figure-level pair organization introduce noise that is unsuitable for high-quality CPT. Specifically, we identify four categories of issues: (1) missing or unrecovered captions for figures whose captions can be recovered from PMC XML; (2) residual XML markup and short-sentence or near-duplicate repetition in captions and figure-referencing contexts; (3) multi-figure context aggregation noise where the same paragraph is redundantly attached to multiple figures; and (4) incoherent context sequences created by concatenating non-adjacent paragraphs from different locations in the article. In addition, BIOMEDICA was not designed for interleaved sample construction. The rich body-text context that references each figure was not incorporated into training samples. We address these issues through the pipeline described below. Figure 1 provides an overview of the complete construction process, moving from raw BIOMEDICA records to caption/context cleanup, interleaved sample construction and refinement, medical relevance and quality classification, modality-aware resampling, and finally PMC-InterCPT.

#### 3.1 Caption and Context Cleanup

We first repair BIOMEDICA entries whose caption field is *No caption found*. For each affected image, we locate the corresponding PMC XML and match the image filename against `<graphic>xlink:href` attributes. When a match is found, we ascend the XML tree until the enclosing `<fig>` or `<table-wrap>` element is reached and extract its descendant caption text. If direct graphic matching fails, we fall back to figure/table identifier matching using common variants such as `fig1`, and `table1`.

We then remove residual XML tags from both captions and image-context fields while preserving their inner text. This step strips common inline markup such as `<xref>`, `<sup>`, `<sub>`, `<bold>`, and `<italic>`, normalizes whitespace, and leaves figure-reference text available for later sample con-

struction. The body-text paragraphs associated with each figure also contain both corpus-level and sample-level repetition. We therefore apply context cleaning at two granularities.

**Within-text repetition cleanup.** Before interleaved construction, we apply sentence-level repetition cleanup to captions and figure-referencing contexts in the article JSON files. This step removes near-adjacent repeated phrases and near-duplicate sentences while preserving panel-specific sentences when their panel labels differ. The short repetitions arise from automatic flattening of XML paragraphs with inline figure references: when nested inline elements are converted to plain text, partial sentence fragments or caption-like spans can appear more than once in the same context string.

**Repeated context removal.** After each context string is cleaned, exact duplicate cleaned contexts are kept only once within the article-level `image_context` map. When the same PMC record appears more than once in the input shards, we build a single cleaned cache entry keyed by PMC ID and reuse it for all copies.

These operations preserve figure-reference anchors whenever possible, because they are needed to identify which additional figures should be co-included in a multi-image sample.

#### 3.2 Interleaved Sample Construction and Refinement

We construct *context-grounded interleaved image-text samples* from the cleaned article JSON files. Each output row contains aligned images and texts arrays, plus a JSON metadata field containing article-level metadata and per-image fields. The sequence alternates image slots with caption/context text slots: each image is followed by its caption, and figure-referencing context paragraphs are appended after the relevant image-caption sequence. The majority of samples contain a single image; multi-image samples arise when a context paragraph references additional figures from the same article.

Two design decisions address the multi-figure aggregation noise identified above. First, when a context paragraph references multiple figures, we detect those references and co-include the corresponding images in the same sample wherever possible, rather than attaching the paragraph redundantly to each figure independently. This preserves cross-figure referential coherence and re-

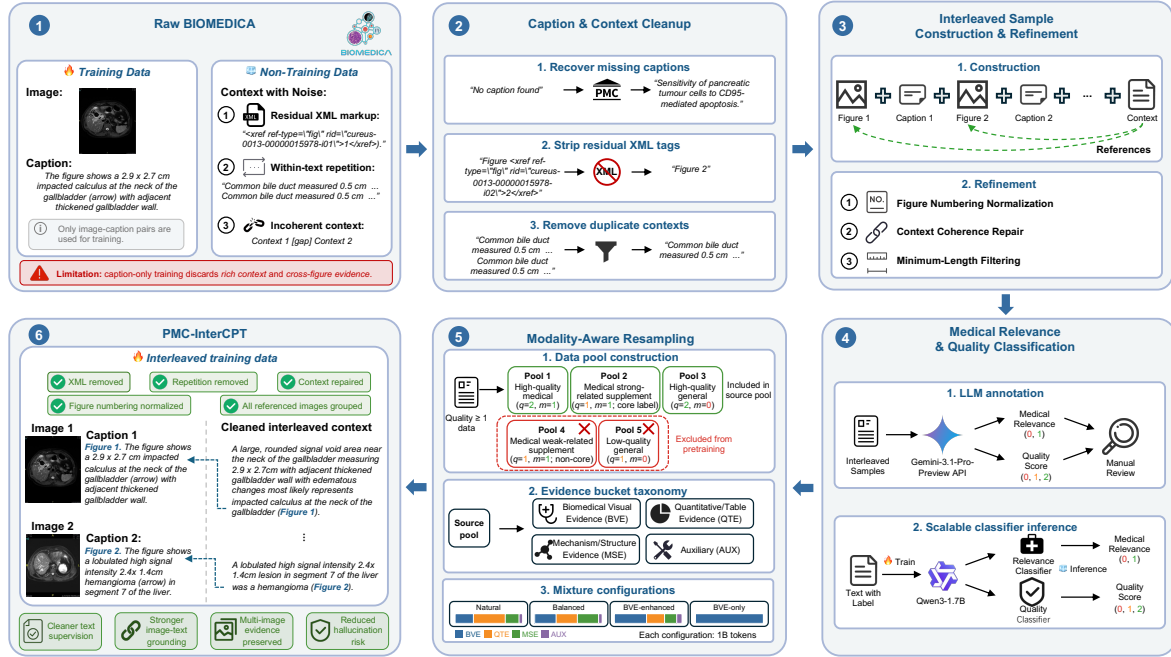


Figure 1: **Overview of the PMC-InterCPT construction pipeline.** Raw BIOMEDICA provides PMC-derived biomedical figures, image-caption pairs, and noisy figure-linked contexts. We clean captions and contexts, construct and refine aligned interleaved samples, filter them with medical relevance and text-quality classifiers, and apply modality-aware resampling to produce the final CPT corpus.

duces hallucination risk. To facilitate accurate cross-figure referencing, we additionally prepend each image’s actual figure number from the source article to its caption text. Second, within a single PMC article, each context string is used at most once during sample expansion, eliminating repeated context across samples constructed from the same article. Finally, we enrich each sample with BIOMEDICA’s per-image metadata, including `image_primary_label`, panel labels, cluster identifiers, and image size, for downstream modality analysis and token accounting.

We apply three sequential refinement steps after initial sample construction.

**Caption numbering normalization.** We infer each figure number from the image identifier or image filename and rewrite caption prefixes into a consistent “Figure *n*.” format. This makes cross-figure references explicit in the interleaved sequence.

**Context coherence repair.** A figure may be referenced by multiple body paragraphs at non-contiguous locations in the paper. For example, once in the Results section and again in the Discussion. Concatenating such paragraphs directly creates an incoherent discourse: there is no natural linguistic transition between paragraphs orig-

inally separated by thousands of words, producing artificial topic jumps that introduce spurious co-occurrence patterns harmful to language model training. To avoid this, we check whether consecutive context segments are adjacent in the article text. When a break is detected, we prefer the segment that references only the primary figure; if both or neither are primary-figure-only, we keep the earlier segment. After pruning context, we remove extra images and captions that are no longer referenced, while always retaining the primary image.

**Length filtering.** Samples below a minimum text threshold are discarded, as they typically lack sufficient context for meaningful CPT signal. For non-Chinese samples, we drop rows with fewer than 12 caption tokens and fewer than 30 context tokens. For samples containing CJK characters, we use character thresholds and drop rows with fewer than 40 caption characters and fewer than 120 context characters.

### 3.3 Medical Relevance and Quality Classification

After sample construction, we filter by medical relevance and text quality using a two-stage approach.

**Stage 1: LLM annotation.** We use gemini-3.1-pro-preview to annotate sampled interleaved records on two dimensions: `medical_relevance`  $\in \{0, 1\}$  and `quality`  $\in \{0, 1, 2\}$ . Annotation is performed with text-only inputs: captions and figure-linked context are provided, while images are withheld. We adopt this design for two reasons. First, in preliminary annotation trials, using images as part of the quality criterion encouraged the annotator model to over-interpret fine visual details or make erroneous visual judgments, introducing hallucination-like noise into labels that were intended to measure corpus quality. Second, because the source records are extracted from PMC articles, the figure-caption and figure-context association is already grounded by the original publication structure. We therefore focus annotation on medical relevance and text purity rather than asking the annotator to re-judge image-text alignment. The quality score measures text purity only, with strict penalties for table dump artifacts, malformed  $\text{\LaTeX}$  fragments, repetitive content, and incoherent text. A score of 2 indicates clean, coherent, low-noise medical text; 1 indicates usable but imperfect text; 0 indicates severe quality problems. We manually review the sampled LLM annotations to remove inconsistent or ambiguous labels before training the scalable classifiers.

**Stage 2: Scalable classifier inference.** We use the reviewed annotations to train separate Qwen3-1.7B classifiers for medical relevance and text quality, and run them over the filtered interleaved corpus with SGLang. The medical classifier outputs a binary score, while the quality classifier outputs a score in  $\{0, 1, 2\}$ . Classifier outputs are joined back to the original Parquet records by `record_id`, and the main data pool keeps records with quality score at least 1. Held-out classifier performance and training details are reported in Appendix D. Briefly, the quality classifier obtains 92.3% accuracy on its balanced held-out test set, while the medical-relevance classifier obtains 93.4% accuracy. For our filtering objective, the most important distinction is separating severely corrupted records from usable ones; accordingly, the quality classifier is strongest on label 0 and label 2, while the middle label 1 remains the expected boundary case between mildly damaged and clean text. This behavior matches the intended use of the labels: quality 0 records are removed, whereas quality 1 records can still contribute useful signal when they are medically

Quality	Medical	Tokens
2	Yes	11.67B
2	No	2.73B
1	Yes	3.69B
1	No	0.69B
0	—	1.02B (filtered)

Table 1: Token distribution after medical relevance and quality classification.

relevant and belong to core biomedical visual categories.

After running inference over the full dataset, we obtain the following token distribution:

### 3.4 Modality-Aware Resampling

**Data pool construction.** After decontaminating against the PMC-VQA benchmark, we partition the  $\text{quality} \geq 1$  data into five pools based on quality score, medical relevance, and image modality: (1) *high-quality medical* (quality=2, medical=1); (2) *medical strong-related supplement* (quality=1, medical=1, label  $\in$  {Clinical Imaging, Immuno Assays, Laboratory Specimens and Cultures, Microscopy, PCR}); (3) *high-quality general* (quality=2, medical=0); (4) *medical weak-related supplement* (quality=1, medical=1, non-core labels); and (5) *low-quality general* (quality=1, medical=0). Pools 4 and 5 are excluded from pretraining: pool 4 contains lower-quality medical samples from weakly related visual categories, while pool 5 contributes off-domain content. The source pool for all subsequent experiments therefore consists of pools 1–3: high-quality medical, medical strong-related supplement, and high-quality general.

**Evidence bucket taxonomy.** Analysis of the natural token distribution within the source pool reveals severe imbalance: Plots and Charts account for 51.2% of tokens, while clinically relevant Clinical Imaging represents only 7.5%. To enable principled resampling, we define four *evidence buckets* that group image modalities by their functional role in biomedical communication:

- **Biomedical Visual Evidence (BVE):** Clinical Imaging, Microscopy, Immuno Assays, PCR, Laboratory Specimens and Cultures
- **Quantitative/Table Evidence (QTE):** Plots and Charts, Tables
- **Mechanism/Structure Evidence (MSE):** Illustrative Diagrams, Chemical Structures,

Config	BVE	QTE	MSE	AUX
Natural dist.	~28%	~52%	~17%	~3%
Balanced	33%	33%	29%	5%
BVE-enhanced	45%	30%	20%	5%
BVE-only	100%	—	—	—

Table 2: Inter-bucket token allocation for the four 1B mixture configurations.

Graphs and Networks, Scientific Formulae and Equations

- **Auxiliary (AUX):** Natural Images, Tools and Materials, Screen Based Visuals, Maps, Ambiguous

**Mixture configurations.** We construct four 1B-token datasets with varying inter-bucket allocation to study the effect of modality distribution (Table 2). Within each bucket, samples are drawn proportionally to their natural token counts unless otherwise specified. For each configuration, we first compute label-level token quotas from the global modality-token distribution, then select records deterministically within each label until the target token budget is reached.

### 3.5 Dataset Scale and Composition

Figure 2 summarizes how the corpus changes across filtering stages and how the final PMC-InterCPT mixture is composed. The raw BIOMEDICA source contains 24.04M samples and 13.65B tokens in its image-caption-oriented format. After interleaved sample construction, the corpus contains 20.16M samples and 19.89B tokens, reflecting the addition of figure-linked body-text context. Minimum-length filtering removes short, weakly grounded samples while preserving most constructed records, yielding 20.02M samples and 19.80B tokens. Quality filtering retains 19.45M samples with quality score at least 1, corresponding to 18.78B tokens, and decontamination against PMC-VQA leaves 19.44M samples and 18.68B tokens. The subsequent pool construction step selects the high-quality medical, strong medical supplement, and high-quality general pools used for mixture construction, resulting in 16.45M source-pool samples and 15.41B tokens. Finally, modality-aware resampling produces PMC-InterCPT with 10.11M samples and 9.63B tokens.

The statistics highlight two aspects of the construction process. First, PMC-InterCPT is smaller than both the quality-filtered pool and full raw

BIOMEDICA in token count, but it concentrates tokens into samples that pass quality filtering, decontamination, and modality-aware source-pool selection. This supports our central hypothesis that continued pretraining benefits more from high-quality, context-grounded interleaved samples than from raw scale alone. Second, the final corpus remains structurally diverse: 13.2% of final samples contain multiple images, which preserves cross-figure evidence that would be unavailable in a caption-only training format. The final label distribution is also not a single-modality corpus: although BVE receives the largest allocation, QTE and MSE together still account for half of the final tokens, maintaining coverage of charts, tables, diagrams, chemical structures, and scientific mechanisms.

## 4 Experiments

### 4.1 Experimental Setup

**Model.** All CPT experiments use Qwen3.5-VL-4B-Base (Qwen Team, 2026) as the backbone. We use the base variant before a fixed SFT stage so that differences primarily reflect the CPT data source and mixture.

**Evaluation.** We evaluate on four medical-oriented benchmarks (MMMU-Med-Test (Yue et al., 2024), MMMU-Pro-Med-10 (Yue et al., 2025), PMC-VQA-clean (Zhang et al., 2023b), and OmniMedVQA (Hu et al., 2024)) and six general or scientific multimodal benchmarks (MMMU-All-Val (Yue et al., 2024), MMMU-Pro-Full-4, MMMU-Pro-Full-10 (Yue et al., 2025), ChartQA (Masry et al., 2022), CharXiv-Val (Wang et al., 2024), and SciVQA (Borisova et al., 2025)). Detailed benchmark descriptions are deferred to Appendix F. For PMC-VQA-clean, we remove all training samples whose source PMC articles overlap with PMC-VQA test questions. ChartQA, CharXiv-Val, and SciVQA are scored using Qwen2.5-72B-Instruct as an LLM judge; all other benchmarks are scored by rule-based option extraction.

**Training protocol.** All experiments use a two-stage CPT+SFT protocol. During CPT, we use a maximum sequence length of 8192 with sequence packing, freeze the ViT encoder, and train for one epoch with cosine learning-rate decay from  $5.0 \times 10^{-6}$  to  $1.0 \times 10^{-6}$ , a warmup ratio of 0.05, micro-batch size 2, and global batch size 256. CPT is run on 64 NVIDIA H800 GPUs. After CPT,

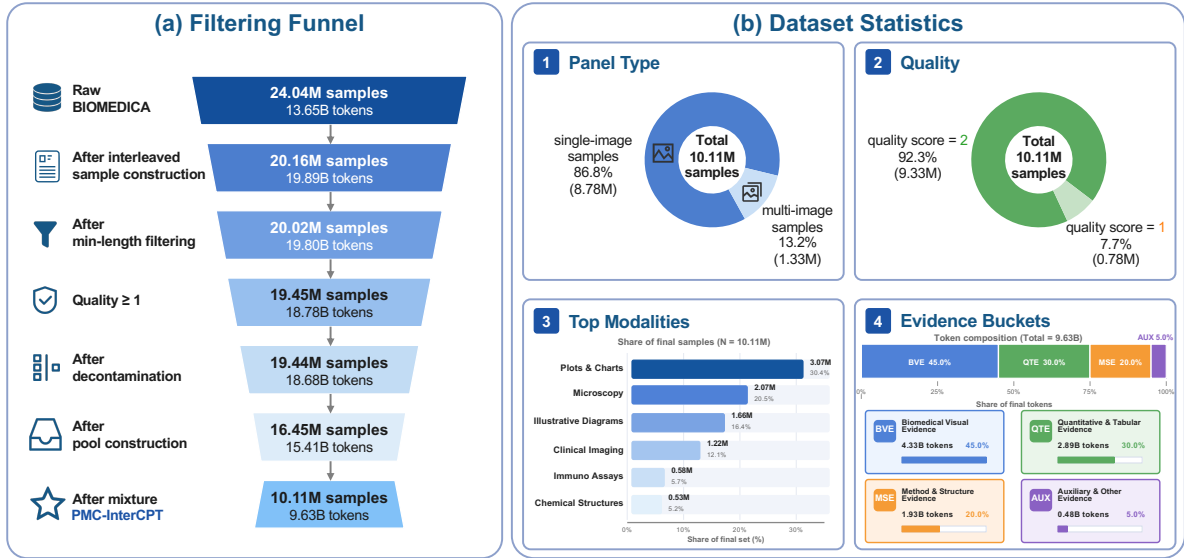


Figure 2: Filtering funnel and final dataset statistics for PMC-InterCPT. (a) The funnel tracks sample and token counts from raw BIOMEDICA through interleaved construction, length filtering, quality filtering, decontamination, source-pool construction, and final mixture sampling. (b) The final mixture is dominated by single-image samples, mostly quality-score-2 records, and follows the BVE-enhanced allocation of 45% BVE, 30% QTE, 20% MSE, and 5% AUX by token count.

all models are supervised fine-tuned on the same 50K examples randomly sampled from LLaVA-OneVision (Li et al., 2024a). During SFT, we train all model parameters for three epochs on 8 NVIDIA H800 GPUs with cosine learning-rate decay from  $2.5 \times 10^{-6}$  to 0, a warmup ratio of 0.1, micro-batch size 2, and global batch size 64.

## 4.2 Main Results: Effect of Data Quality

We compare full-scale CPT on raw BIOMEDICA and PMC-InterCPT, followed by the same fixed SFT stage.

PMC-InterCPT improves over full BIOMEDICA by 1.08 points on the medical average and 1.68 points on the general/scientific average, despite containing fewer CPT tokens. The largest medical gain appears on MMMU-Pro-Med-10 (+2.80), suggesting that the cleaned interleaved contexts and quality filtering are most helpful for harder medical reasoning settings. The gains are not limited to the medical suite: PMC-InterCPT also improves over full BIOMEDICA on ChartQA (+2.00) and CharXiv (+6.10), while recovering much of the degradation observed on MMMU-All and MMMU-Pro-Full after raw BIOMEDICA CPT. PMC-VQA-clean is the only medical benchmark where full BIOMEDICA is slightly higher (-0.15 for PMC-InterCPT), which suggests that our pipeline is not simply overfitting to PMC-style VQA but improves

Metric	Base + SFT	BIOMEDICA	PMC-InterCPT
CPT tokens	–	13.65B	9.63B
MMMU-Med	58.96	58.62	58.73
MMMU-Pro-Med-10	41.61	37.76	40.56
PMC-VQA	61.40	62.90	62.75
OmniMed	85.37	84.97	86.51
Med Avg.	61.84	61.06	<b>62.14</b>
MMMU-All	55.11	53.89	55.00
MMMU-Pro-4	54.80	52.89	53.01
MMMU-Pro-10	43.24	40.58	40.81
ChartQA	75.68	75.00	77.00
CharXiv	53.50	47.90	54.00
SciVQA	68.71	66.74	67.29
Gen Avg.	<b>58.51</b>	56.17	57.85

Table 3: Full-scale CPT+SFT results. All rows use the same 50K-example LLaVA-OneVision SFT stage. Medical average is computed over MMMU-Med-Test, MMMU-Pro-Med-10, PMC-VQA-clean, and OmniMedVQA; general average is computed over the six general/scientific benchmarks. ChartQA, CharXiv, and SciVQA are scored by LLM judge; the other benchmarks use rule-based option extraction.

broader medical and scientific reasoning behavior.

## 4.3 Data Mixture Analysis

### 4.3.1 One-Billion-Token Mixture Configurations

We train four models, each on a distinct 1B-token dataset drawn from the source pool with different inter-bucket allocations (Table 2). We additionally include a raw BIOMEDICA-1B control sampled to

Benchmark	Natural	Balanced	BVE-enh.	BVE-only	BioMed
MMMU-Med	60.10	59.42	59.36	59.82	58.39
MMMU-Pro-Med	41.26	39.86	41.96	39.51	42.66
PMC-VQA	61.10	62.80	61.50	61.75	60.90
OmniMed	86.38	85.56	86.19	86.51	86.04
Med Avg.	62.21	61.91	<b>62.25</b>	61.90	62.00
MMMU-All	55.33	55.44	55.44	54.78	54.78
MMMU-Pro-4	54.16	53.29	53.93	54.16	53.58
MMMU-Pro-10	41.97	42.31	43.12	42.25	43.58
ChartQA	77.08	76.92	76.64	77.20	75.88
CharXiv	53.30	52.60	51.60	51.50	48.20
SciVQA	68.60	68.74	67.45	67.88	66.78
Gen Avg.	<b>58.41</b>	58.22	58.03	57.96	57.13

Table 4: Effect of inter-bucket modality allocation on CPT performance (1B tokens each). BioMed denotes a raw BIOMEDICA-1B control trained with the same CPT and SFT hyperparameters.

the same token budget. All other hyperparameters are held constant.

BVE-enhanced achieves the best medical average among the 1B mixtures and the strongest result on MMMU-Pro-Med-10, while remaining close to the natural mixture on the general/scientific average. The BIOMEDICA-1B control is competitive on the medical average and obtains the highest MMMU-Pro-Med score, but it is consistently weaker on the general/scientific average. All four curated mixtures improve over the BIOMEDICA-1B control on Gen Avg., with the largest gap from the natural mixture (+1.28). This suggests that the cleaned interleaved source pool mainly improves robustness across scientific and chart-oriented benchmarks, while the precise medical gains depend on the downstream benchmark and modality allocation. The general benchmark trend is also consistent with the modality allocation: as the mixture shifts from Natural to Balanced, BVE-enhanced, and BVE-only, the general average gradually decreases. This is expected because the natural mixture contains a larger share of Quantitative/Table Evidence (QTE), which benefits chart- and science-oriented general benchmarks such as CharXiv and SciVQA. At the same time, the detailed results show that increasing BVE is not uniformly harmful to general reasoning: BVE-enhanced improves over Natural on MMMU-All and both MMMU-Pro-Full variants, but loses on CharXiv and SciVQA, where QTE-heavy data is more directly aligned with the benchmark format. These results indicate that modality-aware resampling should be treated as an explicit design trade-off rather than a single universally dominant mixture.

Benchmark	$3 \times 10^{-5}$	$1 \times 10^{-5}$	$5 \times 10^{-6}$
MMMU-Med	57.71	59.42	60.10
MMMU-Pro-Med	37.76	41.96	41.26
PMC-VQA	60.70	60.80	61.10
OmniMed	84.67	84.45	86.38
Med Avg.	60.21	61.66	<b>62.21</b>

Table 5: CPT learning-rate ablation on the natural 1B mixture. All settings use the same fixed SFT stage.

### 4.3.2 CPT Learning Rate

We also compare three CPT learning rates on the natural 1B mixture while keeping the SFT stage fixed. As shown in Table 5, reducing the CPT learning rate from  $3 \times 10^{-5}$  to  $1 \times 10^{-5}$  improves the medical average, and  $5 \times 10^{-6}$  gives the strongest overall result. This supports using a conservative CPT update for domain adaptation: the model benefits from biomedical interleaved data, but an overly large CPT step can degrade the capabilities already present in the base VLM.

## 4.4 Summary

Our experiments reveal two complementary axes of improvement for medical multimodal CPT. First, PMC-InterCPT improves over full raw BIOMEDICA despite using fewer CPT tokens, confirming that structural noise in automatically extracted data actively harms CPT quality. Second, modality-aware resampling (§4.3) provides an explicit way to trade off medical visual evidence against broader chart and scientific reasoning coverage. Together, these results suggest that both data quality and modality distribution deserve explicit optimization attention when building medical multimodal CPT pipelines.

## 5 Conclusion

We presented a systematic pipeline for cleaning and reconstructing context-grounded interleaved image-text data from BIOMEDICA, addressing missing captions, residual XML/text noise, duplicated context, and incoherent multi-paragraph context sequences. Combined with LLM-supervised medical relevance and quality filtering and modality-aware resampling, our pipeline produces PMC-InterCPT, a  $\sim 9.63$ B token high-quality medical multimodal CPT dataset. Experiments on Qwen3.5-VL-4B-Base demonstrate that PMC-InterCPT outperforms full raw BIOMEDICA under the same CPT+SFT protocol, and that evidence-bucket-guided resampling exposes a controllable medical-general trade-

off. Our findings establish data quality and modality distribution as two orthogonal dimensions for medical multimodal CPT optimization.

## Limitations

Our evaluation emphasizes VQA-style benchmarks after a fixed SFT stage, which provides a controlled setting for comparing CPT data sources; broader instruction-following and open-ended generation are natural directions for future evaluation. PMC-InterCPT is currently constructed from English-language PMC articles, and the same reconstruction and filtering pipeline can be extended to multilingual biomedical literature. Finally, the modality mixture ratios we identify are empirically derived on Qwen3.5-VL-4B-Base, while the same evidence-bucket analysis can be revisited for other backbone architectures and target benchmark suites.

## Acknowledgments

This paper is fully supported by a grant from the Research Grants Council of the Hong Kong Special Administrative Region, China (Project No. T41-517/25-N).

## References

- Jean-Baptiste Alayrac, Jeff Donahue, Pauline Luc, Antoine Miech, Iain Barr, Yana Hasson, Karel Lenc, Arthur Mensch, Katherine Millican, Malcolm Reynolds, and 1 others. 2022. Flamingo: a visual language model for few-shot learning. *Advances in Neural Information Processing Systems*, 35:23716–23736.
- Negin Baghbanzadeh, Mohammed Saidul Islam, Sajad Ashkezari, Elham Dolatabadi, and Arash Afkanpour. 2025. Open-pmc-18m: A high-fidelity large scale medical dataset for multimodal representation learning. *arXiv preprint arXiv:2506.02738*.
- Shruthi Bannur, Kenza Bouzid, Daniel C Castro, Anton Schwaighofer, Anja Thieme, Sam Bond-Taylor, Maximilian Ilse, Fernando Pérez-García, Valentina Salvatelli, Harshita Sharma, and 1 others. 2024. MAIRA-2: Grounded radiology report generation. *arXiv preprint arXiv:2406.04449*.
- Ekaterina Borisova, Nikolas Rauscher, and Georg Rehm. 2025. Scivqa 2025: Overview of the first scientific visual question answering shared task. In *Proceedings of the Fifth Workshop on Scholarly Document Processing (SDP 2025)*, pages 182–210.
- Junying Chen, Chi Gui, Ruyi Ouyang, Anningzhe Gao, Shunian Chen, Guiming Hardy Chen, Xidong Wang, Ruifei Zhang, Zhenyang Cai, Ke Ji, Guangjun Yu, Xiang Wan, and Benyou Wang. 2024. HuatuoGPT-Vision, towards injecting medical visual knowledge into multimodal llms at scale. *arXiv preprint arXiv:2406.19280*.
- Xi Chen, Xiao Wang, Soravit Changpinyo, Anthony J Piergiovanni, Piotr Padlewski, Daniel Salz, Sebastian Goodman, Adam Grycner, Basil Mustafa, Lucas Beyer, and 1 others. 2022. Pali: A jointly-scaled multilingual language-image model. *arXiv preprint arXiv:2209.06794*.
- Yutao Hu, Tianbin Li, Quanfeng Lu, Wenqi Shao, Junjun He, Yu Qiao, and Ping Luo. 2024. OmniMed-VQA: A new large-scale comprehensive evaluation benchmark for medical LLM. *Proceedings of the IEEE/CVF Conference on Computer Vision and Pattern Recognition*, pages 22170–22183.
- Hugo Laurençon, Lucile Saulnier, Léo Tronchon, Stas Bekman, Amanpreet Singh, Anton Lozhkov, Thomas Wang, Siddharth Karamcheti, Alexander Rush, Douwe Kiela, and 1 others. 2023. OBELICS: An open web-scale filtered dataset of interleaved image-text documents. *Advances in Neural Information Processing Systems*, 36:71683–71702.
- Bo Li, Yuanhan Zhang, Dong Guo, Renrui Zhang, Feng Li, Hao Zhang, Kaichen Zhang, Peiyuan Zhang, Yanwei Li, Ziwei Liu, and 1 others. 2024a. Llava-onevision: Easy visual task transfer. *arXiv preprint arXiv:2408.03326*.
- Chunyuan Li, Cliff Wong, Sheng Zhang, Naoto Usuyama, Haotian Liu, Jianwei Yang, Tristan Naumann, Hoifung Poon, and Jianfeng Gao. 2023. LLaVA-Med: Training a large language-and-vision assistant for biomedicine in one day. *Advances in Neural Information Processing Systems*, 36:28541–28564.
- Jeffrey Li, Alex Fang, Georgios Smyrnis, Maor Ivgi, Matt Jordan, Samir Gadre, Hritik Bansal, Etash Guha, Sedrick Keh, Kushal Arora, and 1 others. 2024b. DataComp-LM: In search of the next generation of training sets for language models. *Advances in Neural Information Processing Systems*, 37:14200–14282.
- Alejandro Lozano, Min Woo Sun, James Burgess, Liangyu Chen, Jeffrey J Nirschl, Jeffrey Gu, Ivan Lopez, Josiah Aklilu, Anita Rau, Austin Wolfgang Katzer, and 1 others. 2025. Biomedica: An open biomedical image-caption archive, dataset, and vision-language models derived from scientific literature. In *Proceedings of the Computer Vision and Pattern Recognition Conference*, pages 19724–19735.
- Ahmed Masry, Do Long, Jia Qing Tan, Shafiq Joty, and Enamul Hoque. 2022. ChartQA: A benchmark for question answering about charts with visual and logical reasoning. In *Findings of the Association for Computational Linguistics: ACL 2022*, pages 2263–2279.

- Michael Moor, Qian Huang, Shirley Wu, Michihiro Yasunaga, Yash Dalmia, Jure Leskovec, Cyril Zakka, Eduardo Pontes Reis, and Pranav Rajpurkar. 2023. Med-Flamingo: a multimodal medical few-shot learner. In *Machine Learning for Health (MLAH)*, pages 353–367. PMLR.
- Guilherme Penedo, Hynek Kydlíček, Anton Lozhkov, Margaret Mitchell, Colin Raffel, Leandro Von Werra, Thomas Wolf, and 1 others. 2024. The FineWeb datasets: Decanting the web for the finest text data at scale. *Advances in Neural Information Processing Systems*, 37:30811–30849.
- Guilherme Penedo, Quentin Malartic, Daniel Hesslow, Ruxandra Cojocaru, Alessandro Cappelli, Hamza Alobeidli, Baptiste Pannier, Ebtesam Almazrouei, and Julien Launay. 2023. The RefinedWeb dataset for falcon LLM: Outperforming curated corpora with web data, and web data only. *arXiv preprint arXiv:2306.01116*.
- Qwen Team. 2026. [Qwen3.5: Towards native multimodal agents](#). Alibaba Cloud Community Blog.
- Alec Radford, Jong Wook Kim, Chris Hallacy, Aditya Ramesh, Gabriel Goh, Sandhini Agarwal, Girish Sastry, Amanda Askell, Pamela Mishkin, Jack Clark, and 1 others. 2021. Learning transferable visual models from natural language supervision. In *International conference on machine learning*, pages 8748–8763. PmlR.
- Zirui Wang, Mengzhou Xia, Luxi He, Howard Chen, Yitao Liu, Richard Zhu, Kaiqu Liang, Xindi Wu, Haotian Liu, Sadhika Malladi, and 1 others. 2024. Charxiv: Charting gaps in realistic chart understanding in multimodal llms. *Advances in Neural Information Processing Systems*, 37:113569–113697.
- Sang Michael Xie, Hieu Pham, Xuanyi Dong, Nan Du, Hanxiao Liu, Yifeng Lu, Percy S Liang, Quoc V Le, Tengyu Ma, and Adams Wei Yu. 2023. DoReMi: Optimizing data mixtures speeds up language model pretraining. *Advances in Neural Information Processing Systems*, 36:69798–69818.
- Weiwen Xu, Hou Pong Chan, Long Li, Mahani Aljunied, Ruifeng Yuan, Jianyu Wang, Chenghao Xiao, Guizhen Chen, Chaoqun Liu, Zhaodonghui Li, and 1 others. 2025. Lingshu: A generalist foundation model for unified multimodal medical understanding and reasoning. *arXiv preprint arXiv:2506.07044*.
- Xiang Yue, Yuansheng Ni, Kai Zhang, Tianyu Zheng, Ruoqi Liu, Ge Zhang, Samuel Stevens, Dongfu Jiang, Weiming Ren, Yuxuan Sun, and 1 others. 2024. MMMU: A massive multi-discipline multimodal understanding and reasoning benchmark for expert agi. *Proceedings of the IEEE/CVF Conference on Computer Vision and Pattern Recognition*, pages 9556–9567.
- Xiang Yue, Tianyu Zheng, Yuansheng Ni, Yubo Wang, Kai Zhang, Shengbang Tong, Yuxuan Sun, Botao Yu, Ge Zhang, Huan Sun, and 1 others. 2025. Mmmu-pro: A more robust multi-discipline multimodal understanding benchmark. In *Proceedings of the 63rd Annual Meeting of the Association for Computational Linguistics (Volume 1: Long Papers)*, pages 15134–15186.
- Sheng Zhang, Yanbo Xu, Naoto Usuyama, Hanwen Xu, Jaspreet Bagga, Robert Tinn, Sam Preston, Rajesh Rao, Mu Wei, Naveen Valluri, and 1 others. 2023a. BiomedCLIP: a multimodal biomedical foundation model pretrained from fifteen million scientific image-text pairs. *arXiv preprint arXiv:2303.00915*.
- Xiaoman Zhang, Chaoyi Wu, Ziheng Zhao, Weixiong Lin, Ya Zhang, Yanfeng Wang, and Weidi Xie. 2023b. PMC-VQA: Visual instruction tuning for medical visual question answering. *arXiv preprint arXiv:2305.10415*.
- Lianmin Zheng, Liangsheng Yin, Zhiqiang Xie, Chuyue Sun, Jeff Huang, Cody H Yu, Shiyi Cao, Christos Kozyrakis, Ion Stoica, Joseph E Gonzalez, and 1 others. 2024a. Sglang: Efficient execution of structured language model programs. *Advances in neural information processing systems*, 37:62557–62583.
- Yaowei Zheng, Richong Zhang, Junhao Zhang, Yanhan Ye, and Zheyang Luo. 2024b. Llamafactory: Unified efficient fine-tuning of 100+ language models. In *Proceedings of the 62nd annual meeting of the association for computational linguistics (volume 3: system demonstrations)*, pages 400–410.
- Wanrong Zhu, Jack Hessel, Anas Awadalla, Samir Yitzhak Gadre, Jesse Dodge, Alex Fang, Youngjae Yu, Ludwig Schmidt, William Yang Wang, and Yejin Choi. 2023. Multimodal C4: An open, billion-scale corpus of images interleaved with text. *Advances in Neural Information Processing Systems*, 36:8958–8974.

## A Additional Dataset Statistics

### A.1 Raw BIOMEDICA Statistics

BIOMEDICA is built from the PubMed Central Open Access subset and provides an article-level archive serialized into image-caption training records (Lozano et al., 2025). The released corpus contains over 6M full-text articles, over 24M image-caption pairs, and over 30M figure references. Each record includes article-level metadata and image-level annotations, including article identifiers, title, abstract, journal, license, keywords, MeSH terms, citation metadata, image identifiers, image hashes, panel labels, and global/local taxonomy labels. Table 6 summarizes the raw BIOMEDICA properties that are most relevant to our pipeline.

Property	Value
Full-text articles	6M+
Image-caption pairs	24M+
Figure references	30M+
Metadata fields	27
Primary format in BIOMEDICA	Image-caption pairs
Additional signal in our pipeline	Figure-referencing text

Table 6: Raw BIOMEDICA statistics reported by Lozano et al. (2025).

### A.2 Cleaned Dataset Statistics

Table 7 reports the missing-caption recovery statistics. We processed 2,537 tar archives containing 72,151,269 files, including 24,050,423 JSON records. Among these JSON records, 1,987,649 were modified during missing-caption recovery, corresponding to an 8.26% modification rate. For records whose caption field required recovery, 6,238,761 captions were successfully recovered and 3,639,453 were not recovered, giving a success rate of 63.2%. No XML files were missing for the affected articles. Most recovered captions correspond to table-like figure entries whose captions are available in the PMC XML. Unrecovered cases are largely entries such as graphical abstracts, formulae, or other media objects for which the source XML does not provide a caption that can be extracted.

Repeated-text cleanup modified 22,844,977 of 24,050,423 JSON records (94.99%). This high modification rate reflects the prevalence of repeated short fragments and duplicated local context spans

Statistic	Value
Processed tar archives	2,537
Processed files	72,151,269
JSON records	24,050,423
JSON records modified	1,987,649
Modification rate	8.26%
Captions recovered	6,238,761
Captions unrecovered	3,639,453
Recovery success rate	63.2%
Missing XML files	0

Table 7: Missing-caption recovery statistics. The success rate is computed as recovered captions divided by recovered plus unrecovered captions.

introduced when PMC XML paragraphs with inline figure references are flattened into plain text.

Table 8 summarizes the major scale changes across the later pipeline stages. Interleaved construction reduces the number of training records relative to raw BIOMEDICA because it reorganizes article-level figures into context-grounded samples, but increases the token count by adding body-text context. Quality filtering, decontamination, source-pool selection, and final mixture sampling then progressively concentrate the corpus into the final PMC-InterCPT training set.

Stage	Samples	Tokens
Raw BIOMEDICA	24.04M	13.65B
After interleaved construction	20.16M	19.89B
After minimum-length filtering	20.02M	19.80B
Quality score $\geq 1$	19.45M	18.78B
After decontamination	19.44M	18.68B
Source-pool construction	16.45M	15.41B
PMC-InterCPT final mixture	10.11M	9.63B

Table 8: Dataset scale across the main construction stages.

### A.3 Evidence Bucket Distribution

Table 9 reports the evidence-bucket distribution after decontamination and source-pool construction, using the decontaminated global cross statistics. The source pool consists of high-quality medical samples, strong medical supplements from core biomedical labels, and high-quality general samples. Although QTE remains the largest bucket under the natural source-pool distribution, the BVE-enhanced final mixture deliberately increases BVE to 45% of tokens while retaining 30% QTE, 20% MSE, and 5% AUX.

Table 10 reports the final PMC-InterCPT bucket composition after modality-aware resampling. Compared with the natural source-pool distribution,

Evidence bucket	Samples	Text tokens	Image tokens	Total tokens	Source-pool share
Biomedical Visual Evidence (BVE)	4,036,696	2.07B	2.27B	4.33B	28.13%
Quantitative/Table Evidence (QTE)	8,681,434	3.72B	4.30B	8.02B	52.03%
Mechanism/Structure Evidence (MSE)	3,117,352	1.18B	1.37B	2.55B	16.54%
Auxiliary (AUX)	621,590	0.21B	0.30B	0.51B	3.31%
Total	16,457,072	7.18B	8.23B	15.41B	100.00%

Table 9: Evidence-bucket distribution in the decontaminated source pool before final mixture sampling.

the final mixture increases BVE from 28.13% to 45.0% while reducing QTE from 52.03% to 30.0%. This produces a medical-visual-evidence-enhanced corpus while retaining substantial QTE and MSE coverage.

Evidence bucket	Tokens	Final share
BVE	4.33B	45.0%
QTE	2.89B	30.0%
MSE	1.93B	20.0%
AUX	0.48B	5.0%
Total	9.63B	100.0%

Table 10: Final evidence-bucket composition of PMC-InterCPT after modality-aware resampling.

Table 11 gives the corresponding five-pool decomposition. Pools 1–3 are included in the source pool used for all mixture experiments, while pools 4–5 are excluded from pretraining.

Pool	Samples	Tokens
Pool 1: HQ medical	12,389,828	11.67B
Pool 2: Med-strong supp.	782,139	1.02B
Pool 3: HQ general	3,285,105	2.73B
Pool 4: Med-weak supp.	2,278,176	2.61B
Pool 5: Low-quality general	704,879	0.67B

Table 11: Five quality/medical pools after decontamination. HQ denotes high-quality, and supp. denotes supplement. Pools 1–3 form the source pool; pools 4–5 are excluded from pretraining.

## B Sample Construction and Filtering Details

### B.1 Interleaved Sample Format

Each constructed interleaved sample is serialized as a Parquet row with three top-level fields: images, texts, and metadata. The images and texts fields are aligned arrays of equal length. An image slot stores a base64-encoded image in images and null in the corresponding texts position; a text slot stores null in images and the text string in texts. For a single-image sample, the typical

sequence is:

[IMG<sub>1</sub>] → [Figure *n*. caption]  
→ [context paragraph].

For multi-image samples, additional referenced figures are inserted with their captions before the shared context, so that the context can refer to all figures present in the sequence.

The metadata field is a JSON string. It retains article-level fields such as `article_accession_id`, `article_title`, `article_journal`, `article_date`, `article_abstract`, and `article_mesh_terms`, as well as per-image arrays such as `image_file_name`, `image_id`, `image_path`, `caption`, `image_hash`, `image_primary_label`, `panel labels`, `cluster identifiers`, and `image sizes`. Captions are normalized with explicit figure-number prefixes, e.g., Figure 2., to make later context references unambiguous.

### B.2 Context Coherence Repair and Length Filtering

Context coherence repair is applied after initial interleaved sample construction. For samples with multiple context segments, we locate each normalized context string in the full article text and check whether consecutive segments are adjacent in the original article. Two segments are treated as adjacent when their spans are contiguous after whitespace normalization; the implementation also uses an edge-anchor fallback that searches for the concatenation of the previous segment’s ending words and the next segment’s beginning words in the article text.

When two consecutive contexts are not adjacent, we avoid concatenating them into an artificial discourse. The repair rule compares the two segments using raw figure-reference information from the source `image_context`. If only one segment refers exclusively to the primary image, that segment is kept. If both segments are primary-image-only, or neither is primary-image-only, the earlier segment

is kept. After context pruning, images and captions that are no longer referenced by the kept contexts are removed, while the primary image is always retained. The metadata arrays are subsetted consistently with the retained images.

Length filtering is applied after context cleanup. For each row, the first caption and all non-caption context segments are counted separately. The script removes tail figure/table-reference fragments from contexts, normalizes repeated whitespace, collapses duplicated periods, removes empty parentheses, and removes extra spaces before punctuation. Language is determined by detecting CJK characters in the combined caption and context. For Chinese samples, a row is dropped when both `caption_chars < 40` and `context_chars < 120`. For non-Chinese samples, a row is dropped when both `caption_tokens < 12` and `context_tokens < 30`.

## D Medical Relevance and Quality Classification

### D.1 Annotation Guidelines

The LLM annotation step uses text-only inputs: captions and figure-linked context are shown to the annotator, while images are withheld. This design makes the two labels conservative measures of textual usefulness for CPT rather than image-text completeness. One practical reason for this choice is that image-conditioned quality annotation was unstable in our preliminary trials: when images were included as part of the quality criterion, the annotator model sometimes over-interpreted subtle visual details or made incorrect judgments about image content, which introduced hallucination-like errors into labels intended to measure corpus quality. In addition, the raw data are sourced from PMC papers, where the figure, caption, and in-text figure references are linked by the original publication structure. We therefore assume a baseline level of image-text association from the source corpus and restrict annotation to the two aspects that still require scalable filtering: medical relevance and text purity. The annotation contains two targets.

**Medical relevance.** `medical_relevance` is binary. A score of 1 indicates that the sample is medically, clinically, or biomedically relevant, including biomedical research, clinical imaging, pathology, laboratory assays, molecular biology, public health, pharmacology, and other life-science evidence. A score of 0 indicates that the text is not medical or

biomedical, or is only incidentally related to science without useful medical-domain content.

**Text quality.** `quality` is a three-level text-purity score. The score does not measure whether the caption fully describes the image, because the annotator does not receive the image. Instead, it measures whether the text is clean enough to serve as CPT data:

- **0: severe quality problems.** The sample has heavy repetition, copy-paste artifacts, severe garbling, major incoherence, mixed unrelated passages, unreadable table dumps, malformed  $\LaTeX$  source fragments, or text dominated by extraction noise.
- **1: usable but imperfect.** The sample remains mostly understandable, but contains noticeable redundancy, corruption, malformed joins, table-formatting damage, citation clutter, or limited extraction artifacts.
- **2: clean and coherent.** The sample is low-noise, low-redundancy, readable medical or biomedical text with coherent captions and context.

The guidelines deliberately penalize flattened tables and malformed formula extraction. Short, semantically meaningful equations or chemical notation are allowed, but raw source fragments such as `\documentclass`, `\usepackage`, long pasted  $\TeX$  blocks, duplicated rendered/source equations, and broken table rows lower the quality score. If a table or formula artifact is present but limited, the maximum score is usually 1; if it dominates the sample or makes a large section difficult to read, the score is 0.

### D.2 LLM Annotation Prompt

We use `gemini-3.1-pro-preview` with temperature 0 to label sampled interleaved records. The user message concatenates the scoring instruction with a text-only rendering of the sample. The sample rendering separates captions from additional context so that the annotator can distinguish figure captions from body-text evidence. The two highlighted blocks below show the complete scoring instruction and the text-only sample template used in the annotation request.

**System-style instruction used in the annotation request.**

You are grading one interleaved text-only sample for medical multimodal pretraining data filtering.

**Important:**

- You will NOT receive images.
- Judge ONLY from the provided text.
- Do NOT assess completeness because images are unavailable.
- The final quality score is just a text purity score.

**You must score TWO dimensions:**

1. `medical_relevance`: integer in {0,1}
2. `quality`: integer in {0,1,2}

**Definitions:****1) Medical Relevance:**

- 0: not medical / not biomedical / not clinically relevant.
- 1: medically or biomedically relevant.

**2) Quality (text purity only):**

- 0: severe text quality problems. Examples: heavy repetition, obvious copy-paste artifacts, severe garbling, major incoherence, mixed unrelated content, unreadable table dumps, or text dominated by noise.
- 1: usable but imperfect. Some redundancy, corruption, noticeable noise, or table-related formatting damage remains.
- 2: clean, coherent, low-noise, low-redundancy medical text.

**Very strict penalty rules for tables and readability:**

- If the text contains a flattened table, embedded raw table dump, broken row/column listing, mashed cell values, or missing-space table extraction that noticeably hurts readability, quality must be lowered.
- If table artifacts are present but limited and the sample is still mostly readable prose, use quality=1, not 2.
- If table artifacts dominate a substantial portion of the sample, or make a large section hard to read, use quality=0.
- If the text switches from normal prose into malformed table content, this should usually be treated as at least quality=1 and often quality=0 if the malformed part is long or noisy.
- A clean sentence that merely references a table is not a problem. Only penalize when table content itself appears in the text and damages readability.

**Very strict penalty rules for  $\LaTeX$  / formula artifacts:**

- Clean, short, semantically normal mathematical expressions are acceptable and should NOT be penalized by themselves. Examples of acceptable content include inline or display math such as  $(a^2 - 4b = m^2)$ , chemical notation, or brief equations that naturally belong in scientific text.
- Penalize strongly when the text contains malformed, dumped, or extraction-corrupted  $\LaTeX$ / $\TeX$  content that hurts readability. Examples include raw preamble or source fragments such as `\documentclass, \usepackage, \begin{document}, \end{document}`, duplicated rendered formula text, OCR-broken math markup, or long formula-source blocks pasted into prose.
- If a malformed  $\LaTeX$  block appears briefly but the rest of the sample is still understandable, use quality=1.
- If malformed  $\LaTeX$  or formula-source noise occupies a substantial part of the sample, interrupts sentence flow, or makes the sample feel corrupted or unnatural, use quality=0.
- When both a human-readable equation and a dumped  $\LaTeX$  source block appear together, treat this as a formatting artifact and lower quality.

**Other strict penalty rules for quality:**

- Repeated short sentences, repeated clauses, repeated local phrases, or repeated caption fragments should lower quality.
- Context that mostly repeats the caption rather than adding useful text should lower quality.
- Fragmented text, malformed joins, truncation artifacts, broken sentence boundaries, or mixed unrelated passages should lower quality.
- Citation-heavy but still readable text can be acceptable; only penalize if it materially hurts readability or purity.
- Be conservative: if unsure whether table artifacts materially reduce readability, choose the lower quality score.

**Output requirements:**

- Return ONLY one JSON object.
- No markdown, no extra keys.

**Return this exact schema:**

```
{
  "medical_relevance": 0|1,
  "quality": 0|1|2,
  "reasons": {
    "medical_relevance": "one short sentence",
    "quality": "one short sentence"
  }
}
```

**Text-only sample format.**

Sample texts for evaluation:

Captions:

- <caption text for each image>

Additional context texts:

- <figure-linked body-text context>

### D.3 Classifier Training Details

We train two independent Qwen3-1.7B classifiers with LLaMA-Factory (Zheng et al., 2024b): a three-way text-quality classifier and a binary medical-relevance classifier. Both classifiers use full-parameter fine-tuning with the same optimization hyperparameters: `cutoff_len=2048`, `per_device_train_batch_size=4`, `gradient_accumulation_steps=1`, learning rate  $1 \times 10^{-5}$ , 6 epochs, cosine learning-rate schedule, warmup ratio 0.1, and bf16 precision. For each classifier, we select the checkpoint with the best validation-set performance.

Split	Label 0	Label 1	Label 2	Total
Train	408	408	408	1,224
Validation	51	51	51	153
Test	52	52	52	156

Table 12: Balanced split for the quality classifier. Labels 0, 1, and 2 correspond to severe-noise, usable-but-imperfect, and clean text quality.

Split	Label 0	Label 1	Total
Train	1,134	1,134	2,268
Validation	141	141	282
Test	143	143	286

Table 13: Balanced split for the medical-relevance classifier. In the classifier training files, label 0 denotes medical and label 1 denotes non-medical; outputs are converted to the paper’s `medical_relevance` convention during post-processing.

Large-scale classifier inference is run with SGLang (Zheng et al., 2024a). Both classifiers use the same serving configuration: data parallelism 8, tensor parallel size 1, batch size 512, maximum input length 4,096 characters, maximum new tokens 4, and temperature 0. The constrained output space is therefore a single label token for each record.

### D.4 Classifier Test-Set Performance Analysis

Table 14 and Table 15 report held-out test performance for the two classifiers. The quality classifier reaches 92.3% accuracy and 92.3% macro F1. Performance is strongest on label 0 and label 2, with F1 scores of 95.3% and 93.2%, respectively. The lower F1 for label 1 (88.2%) is expected because this middle class is a boundary category: limited table damage, mild repetition, or moderate formatting noise can be close to either severe-noise label

0 or clean label 2. This error pattern is acceptable for filtering because the main data pool keeps quality  $\geq 1$  records; the most important operational distinction is separating severely corrupted samples from usable ones.

Metric	Value
Accuracy	92.3%
Macro F1	92.3%
Label 0 F1	95.3%
Label 1 F1	88.2%
Label 2 F1	93.2%

Table 14: Quality classifier performance on the held-out test set.

The medical-relevance classifier reaches 93.4% accuracy and 93.7% macro F1. The class-level F1 scores are balanced, with 94.2% for medical samples and 93.1% for non-medical samples. This indicates that the classifier is not merely biased toward the dominant biomedical source domain, and can still identify off-domain or weakly related records introduced by broad PMC extraction.

Metric	Value
Accuracy	93.4%
Macro F1	93.7%
Medical label F1	94.2%
Non-medical label F1	93.1%

Table 15: Medical-relevance classifier performance on the held-out test set.

## F Evaluation Details

### F.1 Benchmark Descriptions

MMMU (Yue et al., 2024) is a multi-discipline multimodal reasoning benchmark covering college-level expert subjects. We report MMMU-Med-Test using the Health and Medicine domain, and MMMU-All-Val using the full validation split across disciplines. MMMU-Pro (Yue et al., 2025) is a harder and more robust variant of MMMU with expanded option sets and reduced shortcut cues. We evaluate both the medical subset with 10 options and the full benchmark with 4-option and 10-option configurations.

PMC-VQA (Zhang et al., 2023b) is a medical visual question answering benchmark built from PubMed Central figures. We evaluate a cleaned test split, PMC-VQA-clean, and remove CPT samples whose source PMC articles overlap with this benchmark before training. OmniMedVQA (Hu et al.,

2024) is a broad medical VQA benchmark spanning multiple modalities and question categories, including clinical imaging, pathology, charts, and other biomedical visual evidence.

ChartQA (Masry et al., 2022) evaluates chart understanding through human-written and machine-augmented questions over chart images. CharXiv (Wang et al., 2024) evaluates reasoning over figures from scientific papers, with our experiments using the validation split’s reasoning questions. SciVQA (Borisova et al., 2025) evaluates scientific figure question answering with a mixture of multiple-choice and open-ended questions. Together, these general/scientific benchmarks test whether medical CPT improves biomedical reasoning without collapsing chart, scientific figure, and broad multimodal competence.

## F.2 Evaluation Protocol

All benchmarks are evaluated with zero-shot prompting unless otherwise stated. For multiple-choice questions, the prompt lists the question followed by options and instructs the model to answer directly with the option letter:

```
Question: <question>
Options:
A. <option A>
B. <option B>
...
Answer with the option’s letter from the given
choices directly.
```

For open-ended questions, the prompt is:

```
<question>
Answer the question using a single word or
phrase.
```

Inference uses deterministic decoding with temperature 0. The Medevalkit default generation configuration uses maximum new tokens 1024, top- $p$  0.001, repetition penalty 1.0, presence penalty 2.0.

**Rule-based scoring.** MMMU and MMMU-Pro use exact option-letter accuracy. PMC-VQA-clean and OmniMedVQA use rule-based multiple-choice matching against the gold option letter or answer text. No rule-based score is used for ChartQA, CharXiv-Val, or SciVQA in our reported results.

**LLM-judge scoring.** For ChartQA, CharXiv-Val, and SciVQA, we use Qwen2.5-72B-Instruct as an LLM judge for all reported scores. The judge receives the question, the standard answer, and

the model response, and outputs a binary decision in the format `<judge>0</judge>` for correct or `<judge>1</judge>` for incorrect. The judge prompt treats semantically equivalent answers as correct, which is important for open-ended scientific and chart questions where surface forms can differ from the reference.

## H Additional Results

### H.1 Per-Benchmark and Per-Subset Breakdown

Table 16 provides subject-level results for the two MMMU-style medical benchmarks. PMC-InterCPT recovers much of the performance drop caused by raw BIOMEDICA CPT on the harder MMMU-Pro-Medical-10 setting, improving over BIOMEDICA by 2.80 points overall. The largest gains appear in Pharmacy (+8.77) and Public Health (+8.62), while Diagnostics and Laboratory Medicine also improves over BIOMEDICA on both MMMU-Medical-test and MMMU-Pro-Medical-10. The gains are not uniform across all subjects, which is expected because the final mixture is optimized for broad medical multimodal CPT rather than subject-specific overfitting.

Table 17 reports OmniMedVQA results by question type and image modality. PMC-InterCPT improves most clearly on Disease Diagnosis (+1.94 over BIOMEDICA) and Lesion Grading (+7.10), two categories that require clinically grounded visual interpretation rather than only recognizing the imaging modality. The modality-level results show a similar pattern: PMC-InterCPT improves over BIOMEDICA on CT (+2.19), MR (+2.81), and Fundus Photography (+1.37), while gains are smaller or do not appear for several other modalities. This suggests that the BVE-enhanced mixture strengthens important clinical-imaging categories without uniformly shifting every visual domain.

Table 18 gives additional breakdowns for the scientific and chart-oriented benchmarks. PMC-InterCPT improves ChartQA mainly on the human-written split (+3.52), while the augmented split changes only slightly. On SciVQA, PMC-InterCPT improves open-ended questions (+1.20) but slightly decreases multiple-choice accuracy (-1.08), producing a modest overall gain. The largest scientific-figure improvement appears on CharXiv-Val, where PMC-InterCPT improves every answer-type group and raises the total score by 6.10 points.

Benchmark	Subset	BIOMEDICA	PMC-InterCPT
MMMU-Med	Total	58.62	58.73
MMMU-Med	Basic Medical Science	66.87	67.18
MMMU-Med	Clinical Medicine	62.77	61.23
MMMU-Med	Diagnostics and Laboratory Medicine	46.91	48.77
MMMU-Med	Pharmacy	60.00	63.49
MMMU-Med	Public Health	53.24	50.88
MMMU-Pro-Med-10	Total	37.76	40.56
MMMU-Pro-Med-10	Basic Medical Science	50.00	46.15
MMMU-Pro-Med-10	Clinical Medicine	35.59	32.20
MMMU-Pro-Med-10	Diagnostics and Laboratory Medicine	23.33	26.67
MMMU-Pro-Med-10	Pharmacy	49.12	57.89
MMMU-Pro-Med-10	Public Health	32.76	41.38

Table 16: Per-subset medical benchmark results. Values are accuracies in percent.

Group	Subset	N	BIOMEDICA	PMC-InterCPT
Question	Modality Recognition	11,565	98.66	98.69
Question	Disease Diagnosis	55,387	84.27	86.21
Question	Anatomy Identification	16,448	80.74	81.36
Question	Lesion Grading	2,098	53.00	60.10
Question	Other Biological Attributes	3,498	89.88	91.08
Modality	Fundus Photography	5,398	79.49	80.86
Modality	Microscopy Images	5,680	84.91	84.37
Modality	X-Ray	7,916	87.44	87.41
Modality	Dermoscopy	6,679	83.74	82.45
Modality	CT	15,809	83.90	86.09
Modality	Ultrasound	10,991	80.47	82.08
Modality	MR	31,877	86.07	88.88
Modality	OCT	4,646	95.72	95.61

Table 17: OmniMedVQA breakdown by question type and image modality. Values are accuracies in percent.

Benchmark	Subset	N	BIOMEDICA	PMC-InterCPT
SciVQA	Total	4,200	66.74	67.29
SciVQA	Multiple choice	1,200	70.25	69.17
SciVQA	Open-ended	3,000	65.33	66.53
ChartQA	Total	2,500	75.00	77.00
ChartQA	Human	1,250	63.76	67.28
ChartQA	Augmented	1,250	86.24	86.72
CharXiv-Val	Total	1,000	47.90	54.00
CharXiv-Val	Answer type 1	440	49.55	55.68
CharXiv-Val	Answer type 2	99	63.64	73.74
CharXiv-Val	Answer type 3	232	51.29	57.33
CharXiv-Val	Answer type 4	229	34.50	38.86

Table 18: Scientific and chart-oriented benchmark breakdowns. Values are accuracies in percent.